CYBERNETICS AND PHYSICS, VOL. 8, NO. 1, 2019 , 18–28

NUMERICAL EVALUATION OF SINE-GORDON CHAIN ENERGY CONTROL VIA SUBDOMAINS STATE FEEDBACK UNDER QUANTIZATION AND TIME SAMPLING

Boris Andrievsky
Inst. Problems Mechanical Eng.,
Russian Acad. of Sciences
Saint Petersburg State University
Saint Petersburg, Russia
boris.andrievsky@gmail.com

Yury Orlov
Mexican Scientific Research
Advanced Studies Center
of Ensenada,
Carretera Tijuana-Ensenada,
B.C. 22860, México,
yorlov@cicese.mx

Article history:
Received 01.05.2019, Accepted 12.06.2019

Abstract
The paper is devoted to the numerical performance evaluation of the speed-gradient algorithms, recently developed in (Orlov et al., 2018; Orlov et al., 2019) for controlling the energy of the sine-Gordon spatially distributed systems with several in-domain actuators. The influence of the level quantization of the state feedback control signal (possibly coupled to the time sampling) on the steady-state energy error and the closed-loop system stability is investigated in the simulation study. The following types of quantization are taken into account: sampling-in-time control signal quantization, the level quantization for control, continuous in time; control signal quantization on level jointly with time sampling; control signal transmission over the binary communication channel with time-invariant first order coder; control signal transmission over the binary communication channel with first order coder and time-based zooming; control signal transmission over the binary communication channel with adaptive first-order coder. A resulting impact on the closed-loop performance in question is concluded for each type of the quantization involved.

Key words
energy control, sine-Gordon equation, Speed-gradient, quantization, data rate constraints

1 Introducton

Energy control is motivated by numerous applications in physics and engineering, see [Spong, 1995; Shiriaev *et al.*, 1999; Fantoni *et al.*, 2000; Xin and Kaneda, 2005; Acosta, 2010; Garofalo and Ott, 2017; Fradkov *et al.*, 2018; Tang and Zuo, 2012; Rodriguez *et al.*, 2001; Wang *et al.*, 2003], for mentioning a few. Energy harvesting [Siang *et al.*, 2018; Leong *et al.*, 2018], deployment of tethered systems [Andrievsky and Guzenko, 2014; Nikpoorparizi *et al.*, 2018], quantum control [Boussaid and Caponigro, 2013; Bonnard *et al.*, 2011; Mantile, 2008] are among modern applications which are relevant to energy control as well.

During the last years the energy control problem of spatially distributed systems has been widely studied and proper solutions have been proposed and rigorously justified. In the series of papers the speed-gradient method of [Fradkov and Pogromsky, 1998; Fradkov, 2007; Fradkov *et al.*, 1999] was used to design energy control algorithms for spatially distributed systems, using the boundary control [Dolgopolik *et al.*, 2016; Dolgopolik *et al.*, 2018] and distributed control [Orlov *et al.*, 2017b; Orlov *et al.*, 2017a]. The authors of [Orlov *et al.*, 2017b] analyzed energy control problems for linear wave partial differential equation (PDE) and nonlinear sine-Gordon PDE where the distributed yet uniform over the space control was chosen. The speed-gradient method for energy control of Hamiltonian systems was developed and justified for the above partial differential equations (PDEs). An infinite dimensional version of the Krasovskii–LaSalle principle was validated for the resulting closed-loop systems. By applying this principle, the closed-loop trajectories were shown to either approach the desired energy level set or converge to a system equilibrium. In [Orlov *et al.*, 2017a] a linear wave equation, governing 1-D (one-dimensional) string oscillations, was considered. A distributed control input, independently enforcing the

underlying string over its entire spatial location, was assumed to be available. The speed-gradient method was developed and justified for the considered PDE model. Capabilities of the proposed speed-gradient algorithm of reaching the energy goal were supported by numerical simulations. In [Orlov *et al.*, 2018] an energy control of the sine-Gordon chain driven by several in-domain actuators was considered. The speed-gradient method was generalized to the in-domain actuation such as in [Christofides, 2001; Fridman and Blighovsky, 2012; Fridman and Am, 2013; Pisano and Orlov, 2017] for the purpose of pump/dissipate the energy of the model to a desired level. This result has been extended to control via output feedback by means of developing the Luenberger-type spatial observer, which got measurement data from the sensors, placed within small spatial plant subdomains in [Orlov *et al.*, 2019].

Some important issues have not yet been analytically studied due to nonlinearity and complexity of the systems under consideration. One of the challenging task is to evaluate the closed-loop system performance in the presence of external disturbances and measurement and data transmission errors. The main aim of the paper is obtaining an impression on the limitations of the energy control for a class of nonlinear distributed-parameter physical systems (the sine-Gordon chains) by means of the spatially-discretized control with time and level quantization. In the present work, a step is made for clarifying some of the mentioned issues, namely the effect of level quantization separately, or jointly with a time sampling, is investigated for the control signal applied to the nonlinear chain with the state feedback control, developed in [Orlov *et al.*, 2018].

2 Plant Model and Problem Statement

2.1 Model of Controlled Plant

First, let us briefly recall the key points of [Orlov *et al.*, 2018].

The system of interest is the 1-D chain, described by the following dissipation-free sine-Gordon PDE

$$x_{tt} = \kappa x_{rr} - F_0 \sin x + u(r,t),\ t \geqslant 0, \qquad (1)$$

where t is the time instant, $r \in [0,1]$ is the scalar spatial variable, $x = x(\cdot,t)$ is the instant state of the system, the parameter κ is the elasticity of the system, F_0 stands for the torque gain, $u(r,t)$ is for the manipulable input. The PDE (1) is accompanied with the Dirichlet boundary conditions

$$x(0,t) = 0,\ x(1,t) = 0. \qquad (2)$$

2.2 Sampled-in-space Actuators

The sampled-in-space actuation

$$u(r,t) = \sum_{i=1}^{m} b_i(r) u_i(t) \qquad (3)$$

is in play to control the sine-Gordon model (1) which is thus representable in the form

$$x_{tt} = \kappa x_{rr} - F_0 \sin x + \sum_{i=1}^{m} b_i(r) u_i(t),\ t \geqslant 0. \quad (4)$$

As in [Orlov *et al.*, 2019], the spatial domain $[0,1]$ is uniformly partitioned into $m = 10$ subdomains $[r_i, r_i + h_i]$ of lengths $h_i = 0.1$, $i = 1,\dots,10$ so that $r_i = 0.1(i-1)$. Within each subdomain the corresponding actuator distribution $b_i(r)$ is specified as

$$b_i(r) = \begin{cases} 1, & \text{if} \quad r_i + 0.02 \leqslant r \leqslant r_i + 0.08, \\ 0, & \text{otherwise}, \end{cases} \qquad (5)$$

i.e., the first and the last actuators are located in the distance 0.02 from the left and right boundaries, respectively, whereas the neighboring actuators possessed a slot of the length 0.04 between them.

2.3 Control Objective

The control objective is to pump or dissipate the energy

$$E(x,x_t) = \frac{1}{2} \int_0^1 \Big(x_t^2 + k x_r^2 + 2F_0\big(1 - \cos x\big) \Big)\, dr \quad (6)$$

of the sine-Gordon system (1)–(3) to a prespecified level $E_* \geqslant 0$ for guaranteing the limiting relation

$$\lim_{t\to\infty} E\big(x(\cdot,t), x_t(\cdot,t)\big) = E_* \qquad (7)$$

on the solutions $x(r,t)$ of the closed-loop sine-Gordon model (1), (2).

3 Energy Control Synthesis Using State Feedack

Let us pick-up the goal functional as

$$V(t) = \frac{1}{2}\big(E(t) - E_*\big)^2. \qquad (8)$$

Following the speed-gradient design procedure [Fradkov, 2007; Fradkov *et al.*, 1999], compute the time

derivative of $V(t)$ along the trajectories of system (1), (2), provisionally assuming that $u(r,t)$ is constant on t. Differentiating (8) in time, integrating then the resulting equality by part, and employing a consequence $x_t(0,t) = x_t(1,t) = 0$ of the boundary condition (2) yield [Orlov *et al.*, 2018]

$$\dot{V} = \big(E(t) - E_*\big) \int_0^1 u(r,t) \cdot x_t \, dr. \qquad (9)$$

The control action in [Orlov *et al.*, 2018] is specified in the form of a finite number of sampled-in-space actuators (3). Then $\dot{V}$ reads as

$$\dot{V} = \big(E(t) - E_*\big) \sum_{i=1}^{m} \left(u_i(\cdot) \int_{r_i}^{r_i+h_i} b_i(r) x_t \, dr \right). \quad (10)$$

As the second step of the speed-gradient procedure, one should derive the gradient $\nabla_u \dot{V} \in \mathbb{R}^m$ of the resulting expression of $\dot{V}$ with respect to the control components $u_i(t)$, $i = 1, \ldots, m$, thus arriving at

$$\nabla_u \dot{V} = \big(E - E_*\big) \left[\int_{r_1}^{r_1+h_1} b_1 x_t \, dr \; \ldots \; \int_{r_m}^{r_m+h_m} b_m x_t \, dr \right]^{\mathrm{T}}.$$

The third step of the speed-gradient procedure is to pick up a certain function $\eta(x, x_t)$ which forms an acute angle with $\nabla_u \dot{V}$, i.e., satisfies an inequality $\eta^{\mathrm{T}} \nabla_u \dot{V} \geqslant 0$. In [Orlov *et al.*, 2018], it is chosen in the form

$$\eta(\cdot) = \operatorname{sign}\big(E - E_*\big) \left[\int_{r_1}^{r_1+h_1} b_1 x_t \, dr \; \ldots \; \int_{r_m}^{r_m+h_m} b_m x_t \, dr \right]^{\mathrm{T}}.$$

According to the speed-gradient method, the control action $u(x, \dot{x}) = -\Gamma \eta(x, \dot{x}, t)$ is then constituted with the matrix design parameter $\Gamma = \operatorname{diag}\{\gamma_1, \ldots, \gamma_m\}$, composed of positive entries γ_i, $i = 1, \ldots, m$. Summarizing, the sampled-in-space actuation (3) is specified with

$$u_i(t) = \gamma_i \operatorname{sign} \Delta E(t) \int_{r_i}^{r_i+h_i} b_i x_t \, dr, \qquad (11)$$

where the *energy error* $\Delta E(t) = E_* - E(t)$ is introduced, $i = 1, \ldots, m$.

The present research deals with an *energy dissipation* problem, where desired energy level E_* is set to zero (in other words, the regulation problem is considered). In this particular case, $\Delta E(t) < 0$, therefore $\operatorname{sign} \Delta E = -1$, and control law (11) takes the following form

$$u_i(t) = -\gamma_i \int_{r_i}^{r_i+h_i} b_i x_t \, dr. \qquad (12)$$

4 Numerical Evaluation Setup

4.1 Computational algorithm

Following the previous works [Orlov *et al.*, 2017b; Orlov *et al.*, 2017a; Orlov *et al.*, 2018], in the numerical study, the PDE (1) is discretized in the spatial variable $r \in \mathbb{R}^1$ by uniformly splitting the segment $[0, 1]$ into N sub-intervals. The *discretization step* ν is introduced as $\nu = 1/N$. The resulting system of $N - 1$ ordinary differential equations (ODEs) of the second order are then numerically solved over a time interval $[0, T]$ by applying the medium order variable step Runge–Kutta Method [Dormand and Prince, 1980], performed with the standard MATLAB routine *ode45*.

At the discretization nodes $r_i = i \cdot \nu$, $i = 1, \ldots, N-1$, the second-order spatial derivatives of $x(r,t)$ are approximately computed as

$$x_r(r_i, t) = \frac{x(r_{i+1}, t) - x(r_{i-1}, t)}{2\nu},$$
$$x_{rr}(r_i, t) = \frac{x(r_{i+1}, t) - 2x(r_i, t) + x(r_{i-1}, t)}{\nu^2}.$$

The boundary values $x(r_0, t) = x(r_1, t)$, $x(r_N, t) = x(r_{N-1}, t)$ are specified according to boundary conditions (2), thereby yielding the following values $x(r_0, t) = x(r_N, t) = 0$ at the boundaries. The remaining discrete values $x(r_1, t)$, …, $x(r_{N-1}, t)$ are found by solving $(N - 1)$ ODEs numerically.

To numerically find the values of definite integrals in (12), the MATLAB standard routine *trapz* of the trapezoidal numerical integration are used.

4.2 System Parameters and Initial Conditions

In the simulations of the closed-loop boundary-value problem (1)–(2), (12), the control gains were set to $\gamma_i = \gamma_0 / h_i$, $h_i = m^{-1}$, $i = 1, \ldots, m$ with $\gamma_0 = 5$ and the desired energy level was set to $E_* = 5$. The initial states were pre-specified in the form

$$x(r, 0) = A\big(1 - \cos(2\pi r)\big)^7, \quad x_t(r, 0) = 0 \quad (13)$$

with a certain "magnitude" parameter A. In the present study, $A = 0.02$ is taken. Parameters of (1) were specified to $\kappa = 0.12$, $F_0 = 25$. For avoiding consideration of the various combinations of initial and desired energies, for certainty, the desired energy level $E_* = 0$

is taken, therefore actually, the *stabilization* problem is studied in the present work. The simulation results for various cases of the energy pumping/dissipation may be found in the above mentioned papers [Orlov *et al.*, 2017b; Orlov *et al.*, 2018; Orlov *et al.*, 2019]. For given parameters $\kappa = 0.12$, $F_0 = 25$ and initial conditions (13) with $A = 0.02$, initial system energy $E(0)$ is as $E(0) = 12.47$.

A reasonably high number $N = 2500$ was selected for the PDEs (1) to discretize the spatial variable r and duration of the computation time T was confined to 15.

5 Numerical Results

Below, the several sources of the errors, caused by the discretization and time sampling are numerically studied for the system under consideration. In all of them, discrepancy of the "ideal" control signals given by (12) and the actual ones, denoted by $\tilde{u}_i$, $i = 1, \dots, 10$ is considered as an error source in the examined system.

5.1 Sampled in Time Control Signal

5.1.1 Time Sampling Description In the case of the control signal time sampling, controls $u_i(t)$ are calculated, accordingly to (12) at the uniformly distributed instants $t_k = kT_0$, where constant T_0 is for the given *sampling interval*, $k = 0, 1, \dots$ denotes the step number (the *discrete time*). The resulting signals $u_i(t_k)$ are subjected to the first-order hold procedure which expands $u_i(t_k)$ fixing them over the sampling intervals $[t_k, t_{k+1})$. This leads to the following expression for actuator inputs $\tilde{u}_i$, where $i = 1, \dots, 10$:

$$\tilde{u}_i(t) = u_i(kT_0), \text{ as } kT_0 \leqslant t < (k+1)T_0. \quad (14)$$

5.1.2 Simulation Results for Time Sampling The simulation results in the form of the energy error evolution $\Delta E(t)$, depending on the sampling interval $T_0 \in \{0.01, 0.05, 0.10, 0.20\}$ are plotted on Fig. 1. The logarithmic scale is chosen along the y-axis (for the energy error values). The corresponding values of the steady-state relative energy error $\delta E = \dfrac{\Delta E(t_{\text{fin}})}{\Delta E(0)}$ (in percents) for various time sampling intervals T_0, where $t_{\text{fin}} = 25$ stands for the simulation final time, are collected in Tab. 1.

The results show that the steady-state energy error is negligibly small at least for $T_0 \leqslant 0.10$, but if T_0 exceeds some threshold, loss of stability occurs.

Table 1. Steady-state relative energy error δE (in percents) vs. sampling interval T_0.

T_0	0.01	0.05	0.10	0.20
$\delta E, \%$	$<3.4\cdot10^{-5}$	$7.3\cdot10^{-4}$	0.005	∞

Table 2. Steady-state relative energy error δE (in percents) vs quantization interval δ.

δ	0.01	0.20	0.50
$\delta E, \%$	$5.61 \cdot 10^{-5}$	0.0017	0.0080
δ	1.0	2.0	5.0
$\delta E, \%$	0.0281	0.1215	0.690

5.2 Level Quantization of Control Signal

5.2.1 Quantization Description In this case no time sampling is taken into account, and it is assumed that the control signals

$$\tilde{u}_i = \delta \cdot \left\langle \frac{u_i}{\delta} \right\rangle, \quad i = 1, \dots, 10 \quad (15)$$

are applied to the chain which are results of the uniform quantization of the signals u_i, $i = 1, \dots, 10$ with a given *quantization interval* $\delta > 0$. Hereinafter, $\langle \cdot \rangle$ denotes the `round` function, which rounds each element of the input signal to the nearest integer.

5.2.2 Simulation Results for Level Quantization The simulation results in the form of the energy error evolution $\Delta E(t)$, depending on the quanization interval $\delta \in \{0.01, 0.20, 0.50, 1.0, 2.0, 5.0\}$ are plotted on Fig. 2. The logarithmic scale is chosen along the y-axis (for the energy error values). The plots show that the energy tends in time to a certain steady-state value, depending on the corresponding δ. In Tab. 2, the steady-state relative energy error δE is given (in percents) for various quantization intervals δ, where $t_{\text{fin}} = 25$ stands for the simulation final time.

One may notice that even in the worst case, the steady-state energy error does not exceed 1%. Therefore, simulation results show that the energy is stabilized with an affordable accuracy for the all chosen quantization intervals.

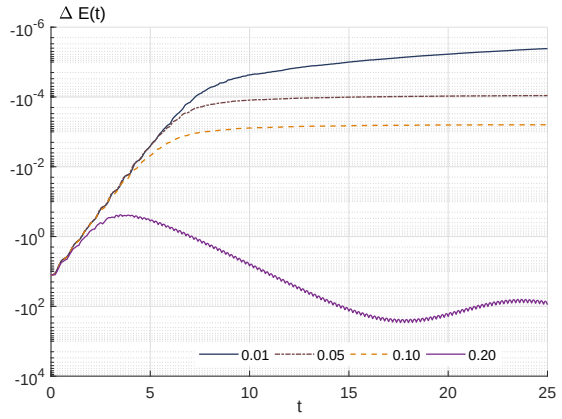

Figure 1. Energy error $\Delta E(t)$: time histories for various values of sampling interval T_0.

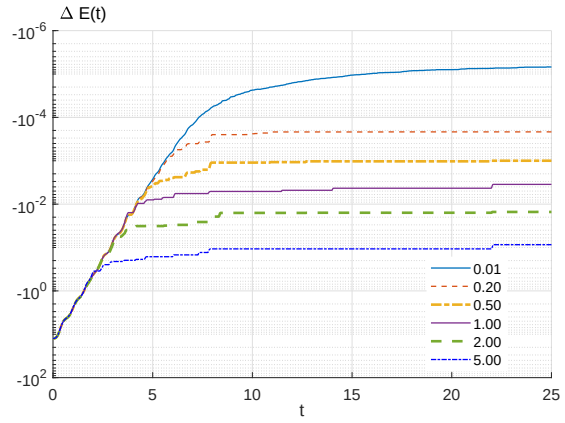

Figure 2. Energy error $\Delta E(t)$: time histories for various values of quantization interval δ.

Table 3. Steady-state relative control error δE (in percents) vs. quantization interval δ for $T_0 = 0.03$.

δ	0.20	0.50	2.0
δE, %	0.00706	0.015	0.127
δ	5.0	10	–
δE, %	0.633	1.92	–

5.3 Control Signal Quantization on Level and Time Sampling

5.3.1 Quantization and Time Sampling Description Consider now the case when both level quantization and the time sampling of the control signal exist in the actuation link. The control signals

$$\tilde{u}_i(t) = \delta \cdot \left\langle \frac{u_i(kT_0)}{\delta} \right\rangle \text{ as } (k-1)T_0 < t \leqslant kT_0,$$

where $i = 1, \ldots, 10$, applied to the chain, are then obtained by zero-order holding of the uniformly quantized signals u_i where constant T_0 denotes the sampling interval, $k = 0, 1, \ldots$ is for the step number (the discrete time).

5.3.2 Simulation Results for Level Quantization and Time Sampling Time histories of the energy error $\Delta E(t)$ for $T_0 = 0.03$ and varying values of the quantization interval $\delta \in \{0.20, 0.50, 2.0, 5.0, 10\}$ are plotted on Fig. 3 in the logarithmic scale for the energy error values. As above, the closed-loop system demonstrate stable performance and the steady-state errors, depending on the quantization interval, occur. The steady-state relative energy errors $\delta E = \dfrac{\Delta E(t_{\text{fin}})}{\Delta E(0)}$ are given in Tab. 3 for various quantization intervals δ and $T_0 = 0.03$. Table 3 shows that the steady-state error is less than 2 for the worst case with $\delta = 10$.

Let us now consider the dependence of the system accuracy on sampling interval T_0 for fixed value of

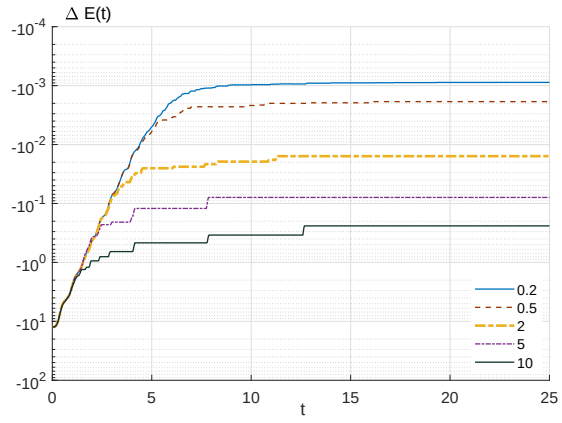

Figure 3. Energy error $\Delta E(t)$: time histories with $T_0 = 0.03$ and varying values of quantization level δ.

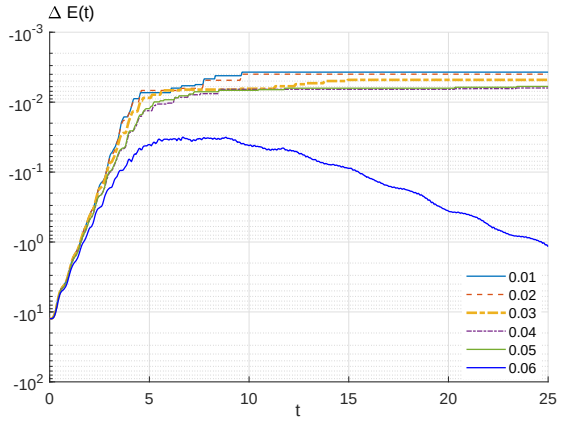

Figure 4. Energy error $\Delta E(t)$: time histories for various values of sampling time T_0 and $\delta = 1$.

Table 4. Steady-state relative controlenergy error δE (in percents) vs. sampling time T_0 for $\delta = 1$.

T_0	0.01	0.02	0.03
δE, %	0.0298	0.0319	0.0385
T_0	0.04	0.05	0.06
δE, %	0.0478	0.0503	∞

δ. Time histories of the energy error $\Delta E(t)$ are depicted on Fig. 4 for various values of sampling interval $T_0 \in \{0.01, 0.02, 0.03, 0.04, 0.05, 0.06\}$ as $\delta = 1$.

The plots of Fig. 4 show that there exists a critical sampling time which should not be exceed to preserve the closed-loop system stability. In the presented example, the transients of the system have approximately the same shape and asymptotically tend to certain steady-state values with the exception of the case $T_0 = 0.06$, where the stability is lost and the process diverges. Table 4 exibits the dependence of the steady state error on sampling time T_0 for $\delta = 1$. As seen, the steady-state error does not depend practically of T_0 and remains negligibly small before the stability is lost.

5.4 Control Signal Transmission Over Binary Communication Channel with Time-invariant First Order Coder

5.4.1 Method Description In this Section, the control signal transmission is considered over the digital communication channel subject to a limiting data transmission rate. It should be noted that performance limitations under constraints, imposed by a finite capacity of communication channel, are well-recognized from the control literature, see [Nair *et al.*, 2007; Andrievsky *et al.*, 2010b; Matveev and Savkin, 2009; Matveev and Pogromsky, 2016] and the references therein.

To begin with, consider the following memoryless (static) *binary* quantizer for a certain signal y:

$$q(y, M) = M \operatorname{sign}(y), \tag{16}$$

where $\operatorname{sign}(\cdot)$ is the *signum* function. Notice that given binary quantizer, each codeword symbol contains one bit of information. This quantizer is a part of the coder with a memory [Nair and Evans, 2003; Liberzon, 2003; Tatikonda and Mitter, 2004; Nair *et al.*, 2007].

Let signal $u(t)$ should be transmitted over the limited capacity communication channel to the actuator. For the *first-order coder* the predicted value $\tilde{u}[k+1] \equiv \tilde{u}\big((k+1)T_0\big)$ is taken equal to $\tilde{u}[k] \equiv \tilde{u}(kT_0)$, see [Tatikonda and Mitter, 2004; Fradkov *et al.*, 2006]. In the coders with a memory, the sequence of *centroids* $c[k]$, $k = 0, 1, \ldots$ with initial condition $c[0] = 0$ is employed. At step k the coder compares the current measured output $u[k] \equiv u(kT_0)$ with value $c[k]$, forming the deviation signal $\partial u[k] = u[k] - c[k]$. Then this signal is discretized with a given *quantizer range* M according to (16). Binary signal

$$s[k] = \operatorname{sign} \partial u[k] \tag{17}$$

is transmitted at step k over the communication channel to the decoder. Then centroid $c[k+1]$ is renewed by the following update algorithm:

$$c[k+1] = c[k] + q\big(\partial u[k], M\big), \quad c[0] = 0. \tag{18}$$

Equations (16)–(18) describe the coder algorithm. The same algorithm is realized by the decoder. Namely, the decoder calculates variable $\tilde{c}[k]$ based on received codeword flow similarly to $s[k]$ and on the value of M which is known on the receiver side.

As obtained in [Andrievsky *et al.*, 2018], in order to avoid the failure of the received signal $\tilde{u}(t)$ to track the transmitted signal $u(t)$, the following inequality

$$M = \alpha L_u T_0 \tag{19}$$

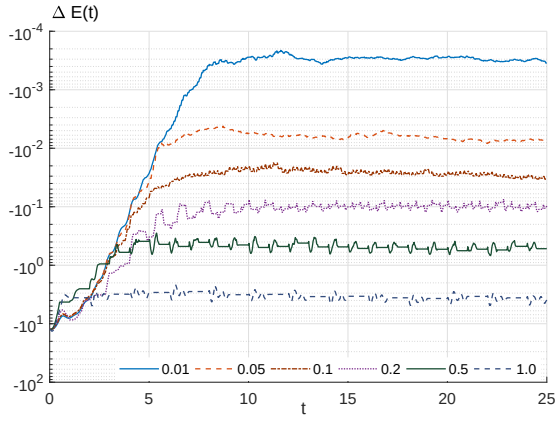

Figure 5. Energy error $\Delta E(t)$: time histories for the binary time-invariant coder with various sampling time T_0.

should be valid for some $\alpha > 1$, where $L_u = \sup_{t \geqslant 0} |\dot{u}(t)|$ is the growth rate of the transmitted signal $u(t)$. In this case, the upper bound of the transmission error $\sup_{t \geqslant 0} |u(t) - \tilde{u}(t)|$ does not exceed $(1+\alpha)L_u T_0$.

5.4.2 Simulation Results for Signal Transmission with Time-invariant First Order Coder The closed-loop system is simulated for various values sampling period T_0. It is worth mentioning that for a binary quantizer (16) the communication channel bit-rate R (in bits per a time unit) is defined as $R = 1/T_0$. This relation makes it possible to calculate the demanded communication channel capacity.

For the present study $L_u = 30$ has been experimentally found by the simulation of the "ideal" control system (1), (2), (6), (12) with the given initial conditions (13). Parameter α in (19) is set to $\alpha = 1.05$.

The simulation results are shown in Fig. 5, where time histories of the energy error $\Delta E(t)$ are depicted for the binary time-invariant coder with various sampling time T_0.

Since the transients do not tend to the steady-state values, the averaged limiting values are used to evaluate the system accuracy. The results are summarized in Tab. 5, where the dependence of the steady-state averaged relative energy error δE on the time sampling interval T_0 and data transmission rate $R = 1/T_0$ (in bits per time unit) is given. These results allow one to conclude that under a data rate less that 2.0 bits per time unit for every control channel $i = 1, \ldots, m$ lead to practically acceptable energy error.

The data transmission scheme described in this section relies upon the Lipschitz constant L_u of $u(t)$. Since the average rate of change for $u(t)$ may vary on time (for example, it differs during the transients and in the steady-state mode, as demonstrated in [Orlov *et al.*, 2017b; Orlov *et al.*, 2017a; Orlov *et al.*, 2018; Orlov *et al.*, 2019]), calculation of M through this constant by means of (19) may be too conservative, reducing

Table 5. Steady-state averaged relative energy error δE vs. time sampling interval T_0 and data transmission rate R.

T_0	0.01	0.05	0.10
R	100	20.0	10.0
δE, %	0.0026	0.0577	2.57
T_0	0.20	0.50	1.00
R	5.0	2.0	1.0
δE, %	0.802	4.17	30.5

the data transmission accuracy. Therefore, when the transient is over, the coder saturation state and consequent failure of the signal transmission may be avoided for less values of M, than are given by (19). Potentially, reducing M on t makes it possible to ensure the asymptotical stabilization of the system. This approach is usually realized in the so-called *zooming* strategy [Brockett and Liberzon, 2000; Liberzon, 2003; Tatikonda and Mitter, 2004; Fradkov *et al.*, 2006; Nair *et al.*, 2007]. The values of $M[k]$ may be precomputed (the *time-based zooming*), or, alternatively, current quantized measurements may be used at each step to update M[k] (the event-based zooming). Time-based zooming is described and evaluated in Sec. 5.5. The event-based zooming, in the form of the *adaptive coding* is considered in Sec. 5.6.

5.5 Control Signal Transmission Over the Binary Communication Channel with First Order Coder and Time-based Zooming

In *time-varying quantizers* [Brockett and Liberzon, 2000; Liberzon, 2003; Tatikonda and Mitter, 2004; Fradkov *et al.*, 2006; Nair *et al.*, 2007] the range M is updated with time and different values of M are used at each step, $M = M[k]$. Using such a "zooming" strategy it is possible to increase coder accuracy in the steady-state mode and at the same time, to prevent coder saturation at the beginning of the process. To this end, the following recursive algorithm for the quantizer range $M[k]$ may be employed

$$M[k] = (M_0 - M_\infty)\rho^k + M_\infty, \quad k = 0, 1, \ldots, \quad (20)$$

where $0 < \rho \leqslant 1$ is the decay parameter, M_∞ stands for the limit value of $M[k]$. M_0 is the initial value of M. Equations (16), (17), (18), (20) describe the coder algorithm. The similar algorithm is realized by the decoder.

5.5.1 Simulation Results for Signal Transmission with First Order Coder and Time-based Zooming

As above, the closed-loop system is simulated for various values sampling period T_0. The coder parameters are taken as follows $M_0 = \alpha L_u T_0$, $M_\infty = 0.05 M_0$,

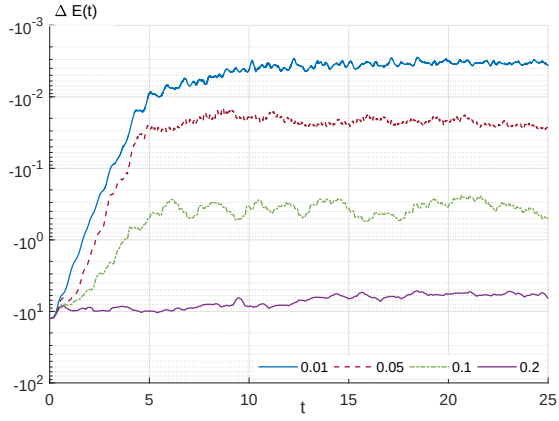

Figure 6. Control error $\Delta E(t)$ time histories for the binary coder with time-based zooming with various sampling time T_0; $s = 0.6$.

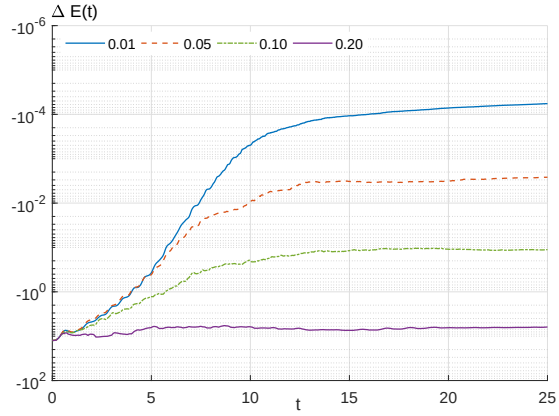

Figure 7. Energy error $\Delta E(t)$: time histories for the binary coder with time-based zooming with various sampling time T_0; $s = 0.15$, $M_\infty = 0$.

$\rho = \exp(-sT_0)$, where $s = 0.6$. The energy error $\Delta E(t)$ time histories for the binary coder with time-based zooming with various sampling time T_0 are depicted in Fig. 6. One may notice that for the considered system an asymptotic stabilization has not been achieved due to non-zero value of M_∞. The case of $M_\infty = 0$ and $s = 0.15$ is depicted in Fig. 7. The simulation results in the form of dependence of the steady-state averaged relative control error δE on time sampling interval T_0 and data transmission rate $R = 1/T_0$ (in bits per time unit) are summarized in Tabs. 6, 7.

5.6 Control Signal Transmission Over the Binary Communication Channel with Adaptive First-order Coder

The following *adaptive coding* procedure may be employed. It assumes adaptively changing quantizer range $M[k]$ depending on the current measurements, cf. [Goodman and Gersho, 1974; Andrievsky *et al.*, 2010a; Gomez-Estern *et al.*, 2011; Goodwin *et al.*, 2012; Andrievsky, 2013]. Range $M[k]$ in (16)–(18) is updated adaptively by means of the following proce-

Table 6. Steady-state averaged relative energy error δE vs. time sampling interval T_0 and data transmission rate R for the coder with a time-based zooming; $s = 0.6$, $M_\infty = M_0/20$.

T_0	0.01	0.05	0.10
R	100	20.0	10.0
δE, %	0.0273	0.2149	3.85

Table 7. Dependence of the steady-state averaged relative control error δE on time sampling interval T_0 and data transmission rate R for the coder with a time-based zooming; $s = 0.6$, $M_\infty = 0$.

T_0	0.01	0.05	0.10
R	100	20.0	10.0
δE, %	$< 4.57 \cdot 10^{-4}$	0.021	0.906

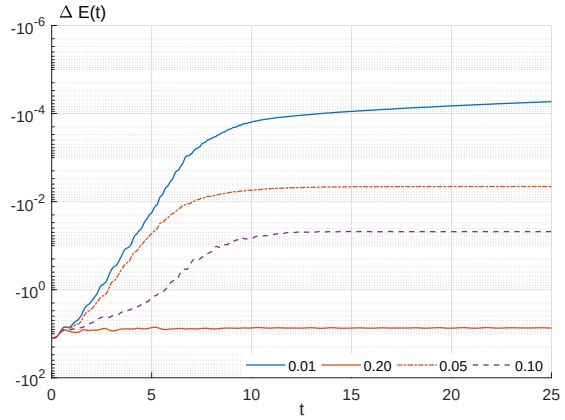

Figure 8. Energy error $\Delta E(t)$: time histories for the binary adaptive coder with $M_\infty = 0$ and various sampling time T_0; $s = 0.6$.

dure:

$$\lambda[k] = (s[k] + s[k-1] + s[k-2])/3,$$
$$s[-1] = 0,\ s[-2] = 0,$$
$$M[k+1] = M_\infty + \begin{cases} \rho M[k], & \text{as } |\lambda[k]| \leqslant 0.5, \\ M[k]/\rho, & \text{otherwise,} \end{cases}$$
$$M[0] = M_0,$$

where M_0 stands for the initial value of $M[k]$, M_∞ denotes the lower admissible bound of M.

5.6.1 Simulation Results for Signal Transmission with First Order Adaptive Coder The closed-loop system is simulated for various values of the sampling period T_0. The coder parameters are taken as follows $M_0 = \alpha L_u T_0$, $M_\infty = 0$, $\rho = \exp(-sT_0)$, where $s = 0.6$. The time histroies of the energy error $\Delta E(t)$ are depicted in Fig. 8. An impression of $M[k]$ adjustment along with the control action time history for $T_0 = 0.1$ may be obtained from the plots, shown in Fig. 9. The simulation results show that the adaptive coding procedure ensures the smooth transients with a relatively high steady-state accuracy.

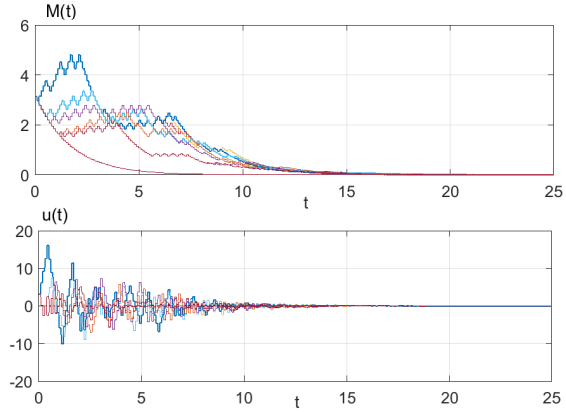

Figure 9. Time histories of quantizer range $M(t_k)$ (upper plot) and control action $\tilde{u}(t)$ (lower plot) for binary adaptive coder with $M_\infty = 0$ and sampling time $T_0 = 0.1$; $s = 0.6$.

Table 8. Steady-state averaged relative energy error δE vs. time sampling interval T_0 and data transmission rate R binary adaptive coder with $M_\infty = 0$; $s = 0.6$.

T_0	0.01	0.05	0.10
R	100	20.0	10.0
δE, %	$< 4.33 \cdot 10^{-4}$	0.0577	2.57

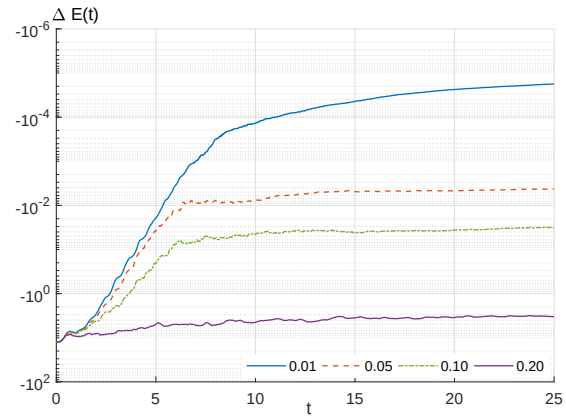

Figure 10. Energy error $\Delta E(t)$: time histories for the binary adaptive coder with $M_\infty = 0$ and various sampling time T_0; $s = 0.15$.

Table 9. Steady-state averaged relative energy error δE vs. time sampling interval T_0 and data transmission rate R for the binary adaptive coder with $M_\infty = 0$; $s = 0.15$.

T_0	0.01	0.05	0.10
R	100	20.0	10.0
δE, %	$< 1.44 \cdot 10^{-4}$	0.0343	0.257

In Tab. 8, the dependence of the steady-state averaged relative control error δE on the time sampling interval T_0 and data transmission rate $R = 1/T_0$ (in bits per time unit) is presented for the adaptive coder.

The time histories of $M[k]$ and control action $u(t)$ are

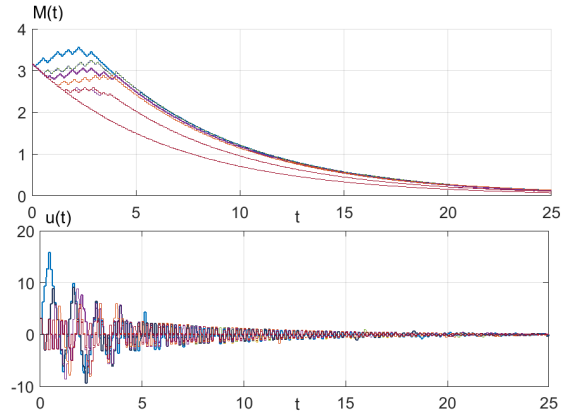

Figure 11. Time histories of the quantizer range $M(t_k)$ (upper plot) and control action $\tilde{u}(t)$ (lower plot) for binary adaptive coder with $M_\infty = 0$ and sampling time $T_0 = 0.1$; $s = 0.15$.

shown in Fig. 11 for the system with the adaptive coder and $s = 0.15$, $T_0 = 0.1$.

6 Conclusions

In the paper, an impression on the limitations of the energy control for the sine-Gordon chains by means of the spatially-discretized control with time and level quantization is obtained. The speed-gradient-based state feedback energy control, developed in [Orlov *et al.*, 2018; Orlov *et al.*, 2019], is numerically evaluated for a sine-Gordon spatially distributed system. The closed-loop system robustness is investigated under various types of disturbances, caused by: sampling-in-time control signal quantization, the level quantization for control, continuous in time; control signal quantization on level jointly with time sampling; control signal transmission over the binary communication channel with time-invariant first order coder; control signal transmission over the binary communication channel with first order coder and time-based zooming; control signal transmission over the binary communication channel with adaptive first-order coder. The results obtained demonstrate robustness of the examined regulation algorithm with respect to the considered disturbances. The steady-state error dependence on the quantization/sampling parameters is numerically evaluated by the simulations. Particularly, it is shown that the most critical role is played by the time sampling, which may lead to loss of the system stability once a certain threshold is overcome.

In the future it is planned to expand this study on the output-feedback energy control systems of [Orlov *et al.*, 2019] where both the control and measurement signals may be affected by the quantization, and to evaluation of non-discontinuous type speed gradient control algorithms. Numerical study of robustness in the presence of quantization disturbances and extension to non-collocated actuation and sensing of other nonlinear distributed parameter models, e.g., Klein-Gordon PDE and chains [Dolgopolik *et al.*, 2018; Kovaleva, 2016] are among challenges to be tackled within the adopted framevork.

Acknowledgment

This work was partly supported by the RFBR (Grants 17-08-01728, 18-38-20037) and CONACYT (Grant A1-S-9270).

The authors also wish to thank Professor Alexander Fradkov for his motivating discussions of the present investigation.

References

Acosta, J.Á. (2010). Furuta's pendulum: A conservative nonlinear model for theory and practise. *Mathematical Problems in Engineering*.

Andrievsky, B. (2013). Information transmission based on adaptive synchronization of chaotic Lorenz systems over the digital communication channel. *Cybernetics and Physics* **1**, 10–14.

Andrievsky, B., A. L. Fradkov and D. Liberzon (2018). Robustness of Pecora–Carroll synchronization under communication constraints. *Systems & Control Letters* **111**, 27–33.

Andrievsky, B., A. L. Fradkov and D. Peaucelle (2010*a*). Estimation and control under information constraints for LAAS helicopter benchmark. *IEEE Trans. Contr. Syst. Technol.* **15**(5), 1180–1187.

Andrievsky, B. and P.Yu. Guzenko (2014). Energy speed-gradient control of nonlinear satellite oscillations. *Cybernetics And Physics* **3**(1), 9–15.

Andrievsky, B. R., A. S. Matveev and A. L. Fradkov (2010*b*). Control and estimation under information constraints: Toward a unified theory of control, computation and communications. *Autom. Remote Control* **71**(4), 572–633.

Bonnard, B., J.-B. Caillau and O. Cots (2011). Energy minimization in two-level dissipative quantum control: The integrable case. *Discrete And Continuous Dynamical Systems* **31, supplement S**, 198–208.

Boussaid, N. and T. Caponigro, M.and Chambrion (2013). Total variation of the control and energy of bilinear quantum systems. In: *Proc. 52nd IEEE Conference on Decision and Control (CDC 2013)*. pp. 3714–3719.

Brockett, R. W. and D. Liberzon (2000). Quantized feedback stabilization of linear systems. *IEEE Trans. Automat. Contr.* **45**(7), 1279–1289.

Christofides, P.D. (2001). *Nonlinear and Robust Control of PDE Systems: Methods and Applications to Transport-Reaction Processes*. Birkhäuser. Boston.

Dolgopolik, M., A. L. Fradkov and B. Andrievsky (2018). Boundary energy control of a system governed by the nonlinear Klein–Gordon equation. *Math. Control Signals Syst.*

Dolgopolik, M., A.L. Fradkov and B. Andrievsky

(2016). Boundary energy control of the sine-Gordon equation. *IFAC-PapersOnLine* **49**(14), 148–153.

Dormand, J. R. and P. J. Prince (1980). A family of embedded Runge-Kutta formulae. *J. Comp. Appl. Math.* **6**, 19–26.

Fantoni, I., R. Lozano and M.W. Spong (2000). Energy based control of the pendubot. *IEEE Trans. Automat. Contr.* **45**(4), 725–729.

Fradkov, A. L. (2007). *Cybernetical Physics. From Control of Chaos to Quantum Control*. Springer.

Fradkov, A. L. and A. Yu. Pogromsky (1998). *Introduction to control of oscillations and chaos*. World Scientific Pub. Co. Singapore.

Fradkov, A. L., B. Andrievsky and R. J. Evans (2006). Chaotic observer-based synchronization under information constraints. *Physical Review E* **73**, 066209.

Fradkov, A. L., I. V. Miroshnik and V. O. Nikiforov (1999). *Nonlinear and Adaptive Control of Complex Systems*. Kluwer. Dordrecht.

Fradkov, A.L., S. Lashkov and B. Andrievsky (2018). Energy synchronization of pendulum mechanisms. In: *Proc. 15th Intern. Conf. Control, Automation, Robotics and Vision, (ICARCV 2018), Singapore*. IEEE. pp. 1257–1262.

Fridman, E. and A. Blighovsky (2012). Robust sampled-data control of a class of semilinear parabolic systems. *Automatica* **48**(5), 826–836.

Fridman, E. M. and N. Bar Am (2013). Sampled-data distributed H_∞ control of transport reaction systems. *SIAM J. Control and Optimization* **51**(2), 1500–1527.

Garofalo, G. and C. Ott (2017). Energy based limit cycle control of elastically actuated robots. *IEEE Trans. Automat. Contr.* **62**(5), 2490–2497.

Gomez-Estern, F., C. Canudas de Wit and F. Rubio (2011). Adaptive delta modulation in networked controlled systems with bounded disturbances. *IEEE Trans. Automat. Contr.* **56**(1), 129–134.

Goodman, D. J. and A. Gersho (1974). Theory of an adaptive quantizer. *IEEE Trans. Commun.* **COM-22**(8), 1037–1045.

Goodwin, G.C., K. Lau and M.G. Cea (2012). Control with communication constraints. In: *Proc. 12th Int. Conf. on Control Automation Robotics & Vision (ICARCV 2012)*. IEEE. Guangzhou, PRC. pp. 1–10.

Kovaleva, A. (2016). Autoresonance in Klein-Gordon chains. *Cybernetics And Physics* **5**(4), 123–129.

Leong, A. S., S. Dey and D. E. Quevedo (2018). Transmission scheduling for remote state estimation and control with an energy harvesting sensor. *Automatica* **91**, 54–60.

Liberzon, D. (2003). Hybrid feedback stabilization of systems with quantized signals. *Automatica* **39**, 1543–1554.

Mantile, A. (2008). Point interaction controls for the energy transfer in 3-D quantum systems. *Intern. J. Control* **81**(5), 752–763.

Matveev, A. and A. Pogromsky (2016). Observation of nonlinear systems via finite capacity channels: Constructive data rate limits. *Automatica* **70**, 217–229.

Matveev, A. S. and A. V. Savkin (2009). *Estimation and Control over Communication Networks*. Birkhäuser. Boston.

Nair, G. N. and R. J. Evans (2003). Exponential stabilisability of finite-dimensional linear systems with limited data rates. *Automatica* **39**, 585–593.

Nair, G. N., F. Fagnani, S. Zampieri and R.J. Evans (2007). Feedback control under data rate constraints: an overview. *Proc. IEEE* **95**(1), 108–137.

Nikpoorparizi, P., N. Deodhar and C. Vermillion (2018). Modeling, control design, and combined plant/controller optimization for an energy-harvesting tethered wing. *IEEE Trans. Contr. Syst. Technol.* **26**(4), 1157–1169.

Orlov, Y., A. Fradkov and B. Andrievsky (2019). Output feedback energy control of the sine-Gordon pde model using collocated spatially sampled sensing and actuation. *IEEE Trans. Automat. Contr.* (to appear).

Orlov, Y., A. L. Fradkov and B. Andrievsky (2017*a*). Sliding mode-based speed-gradient control of the string energy. *IFAC PapersOnLine* **50**(1), 8484–8489.

Orlov, Y., A.L. Fradkov and B. Andrievsky (2017*b*). Energy control of distributed parameter systems via speed-gradient method: case study of string and sine-Gordon benchmark models. *Intern. J. of Control* **90**(11), 2554–2566.

Orlov, Y., A.L. Fradkov and B. Andrievsky (2018). In-domain energy control of the sine-Gordon model. In: *Proc. 2018 European Control Conference (ECC 2018), Limassol, Cyprus*. IEEE. pp. 3019–3024.

Pisano, A. and Y. Orlov (2017). On the ISS properties of a class of parabolic DPS with discontinuous control using sampled-in-space sensing and actuation. *Automatica* **81**, 447–454.

Rodriguez, H., R. Ortega and G. Escobar (2001). A new family of energy-based non-linear controllers for switched power converters. In: *Proc. 2001 IEEE Intern. Symp. Industrial Electronics, Pusan, South Korea*. Vol. 2. IEEE. pp. 723 – 727. (Cat. No. 01TH8570).

Shiriaev, A.S., H. Ludvigsen and O. Egeland (1999). Swinging up of the spherical pendulum. *IFAC Proceedings Volumes* **32**(2), 2193–2198. Proc. 14th IFAC World Congress, Beijing, China, 1999, 5-9 July.

Siang, J., M.H. Lim and Leong M.S. (2018). Review of vibration-based energy harvesting technology: Mechanism and architectural approach. *Intern. J. Energy Research*.

Spong, M. (1995). The swing up control problem for the acrobot. *IEEE Control Syst. Mag.* **15**(1), 49–55.

Tang, X. and L. Zuo (2012). Simultaneous energy harvesting and vibration control of structures with tuned mass dampers. *J. Intelligent Material Systems and Structures* **23**(18), 2117–2127.

Tatikonda, S. and S. Mitter (2004). Control under

communication constraints. *IEEE Trans. Automat. Contr.* **49**(7), 1056–1068.

Wang, Y., D. Cheng, C. Li and Y. Ge (2003). Dissipative Hamiltonian realization and energy-based-disturbance attenuation control of multimachine power systems. *IEEE Trans. Automat. Contr.* **48**(8), 1428–1433.

Xin, X. and M. Kaneda (2005). Analysis of the energy-based control for swinging up two pendulums. *IEEE Trans. Automat. Contr.* **50**(5), 679–685.